Key Engineering Materials
ISSN: 1662-9795, Vol. 926, pp 1949-1958
doi:10.4028/p-oxs247

Submitted: 2021-12-01
Revised: 2022-01-24
Accepted: 2022-01-28
Online: 2022-07-22

Numerical and Experimental Investigations on the Mechanical Properties of Milled Specimens from an AA7020 Tube

Jonas Reblitz[1,a*], Franz Reuther[2,b], Ricardo Trân[2,c], Verena Kräusel[2,d] and Marion Merklein[1,e]

[1]Institute of Manufacturing Technology, Friedrich-Alexander-Universität Erlangen-Nürnberg, Egerlandstraße 13, 91058 Erlangen, Germany

[2]Fraunhofer Institute for Machine Tools and Forming Technology, Reichenhainer Straße 88, 09126 Chemnitz, Germany

[a]jonas.reblitz@fau.de, [b]franz.reuther@iwu.fraunhofer.de, [c]ricardo.tran@iwu.fraunhofer.de, [d]verena.kraeusel@mb.tu-chemnitz.de, [e]marion.merklein@fau.de

*Corresponding author

Keywords: Material characterization, W-temper condition, tensile test, tubes

Abstract. The reduction of weight is crucial in the automotive sector to reach a lower energy consumption and an increased range, especially for electrically powered vehicles. In this regard, body-in-white parts offer a high potential for the application of lightweight construction. The required weight savings can be achieved by implementing parts with a high strength-to-weight ratio. A promising approach is the combination of lightweight materials and lightweight design, which can be realized by tubular components made of high strength aluminum. Due to their structural stiffness and high crashworthiness, those structures are often used as safety-relevant car body components. However, the material characterization of tube profiles is a major challenge, which in turn impedes an accurate numerical simulation and precise process design. In contrast to flat semi-finished parts, various effects of the production process and the geometry, regarding the stress state under load, must be taken into account. For this purpose, adapted testing methods considering the geometrical and mechanical properties of the tubular parts have to be investigated, in order to generate an accurate material model and process design. Within this research work, tubular components made out of AA7020 in W-temper condition were used to analyze the mechanical properties. In this regard, several tensile specimens are milled from a tube, so they also have a curvature profile. The experimental tensile tests have been performed at different strain rates by using a universal testing machine from type Gleeble 3500. To ensure a proper measurement of the mechanical properties, the clamping jaws of the testing machine are adjusted to the curved samples. The investigated material parameters are subsequently transferred to an FE model with curved specimen to enable an accurate prediction of the forming behavior. In addition, an FE model of a flat tensile specimen was also created for comparison, in order to gain a profound knowledge regarding the influence of the geometric and mechanical properties of tubular components.

1. Introduction

One current global challenge is the reduction of carbon dioxide emissions and energy consumption. Especially the transporting sector has a significant impact with a share of 21 % on the total carbon dioxide emissions in the EU [1]. It is also the only sector with higher greenhouse gas emissions than in 1990 [2]. This development is caused by the continuous increase in vehicle weight and the associated rise in engine power as well as the growing level of urban traffic [3]. An important measure for reducing the energy consumption is the utilization of lightweight construction. Therefore, materials with a high strength-to-weight ratio are used, such as high strength aluminum alloys of the 7xxx series. An additional weight reduction can be achieved by the application of tube profiles. Further processing based on hydroforming enables the realization of the required complex part geometries for tailored components. Due to their high structural stiffness and crashworthiness, profile components are often used as safety-relevant car body components [4]. However, process

understanding and methods for an accurate material characterization are missing. In this context, process-related testing methods considering the geometrical and mechanical properties of the tubular parts have to be investigated, in order to enhance the process understanding and the numerical process design. For this purpose, the mechanical properties of tubular semi-finished parts milled out of the aluminum alloy AA7020 are investigated by means of experiments and FE-simulations. For the characterization of the material properties, micro hardness measurements and optical analysis have been performed. The mechanical behavior is subsequently specified by tensile tests whereby suitable methods for the sample preparation and testing are analyzed. To enhance the formability of high strength aluminum alloys the specimens are heat-treated and tested in W-temper condition. The investigated material data is transferred to a numerical simulation for a deeper analysis. By the comparison of the stress and strain states between a flat and a curved specimen the influence of the sample geometry on the mechanical properties is evaluated. The results are used to determine the suitability of the investigated method for the characterization of tube profiles.

2. Methodology

Preparation of tensile specimens from a tube. For an appropriate and process-related characterization of the material properties, tensile specimens are milled from a tube by a CNC milling machine. Therefore, the semi-finished products with a diameter of 60 mm are clamped on one side for machining the contour of the samples shown in Fig. 1 a). The specimens are subsequently cut out of the tube. Due to the high surface quality and the negligible heat input, no further processing of the cutting edges is necessary. The resulting sample geometry is schematically shown in Fig. 1 b).

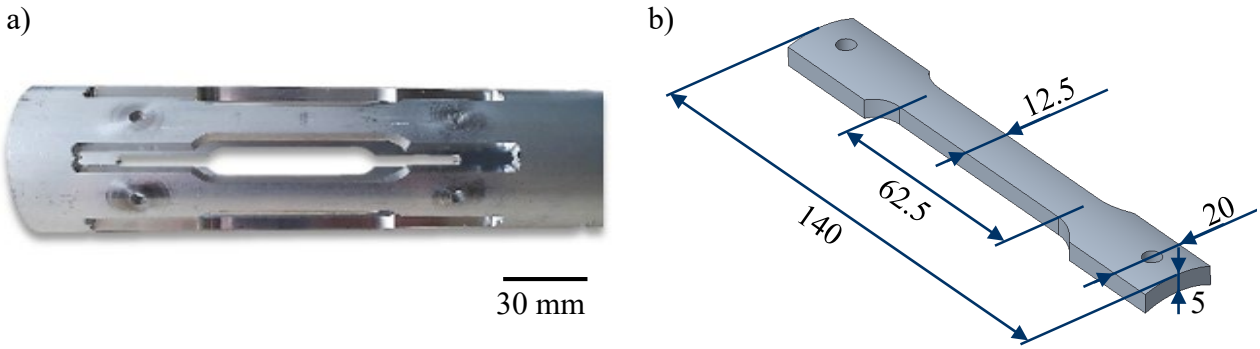

Fig. 1: a) Specimen preparation and b) investigated geometry, derived from conventional tensile specimens

The sample geometry is an adapted version of an A50 specimen according to ISO 6892-1 for the testing with the thermo-mechanical simulator Gleeble 3500. It is characterized by a testing area with a length of 62.5 mm, a width of 12.5 mm and a tube wall thickness of five millimeters. Two drillings with a diameter of 5.2 mm are applied for a central positioning in the clamping jaws.

Experimental setup of the tensile test. The clamping jaws are adapted to the curvature of the tensile specimens, as shown in Fig. 2 a). Thus, undesired stress and strain at the clamping by flattening the bar ends is avoided. By integrating the clamping jaws into the thermo-mechanical simulator of type Gleeble 3500, tensile tests with specific temperature profiles up to 1700 °C can be performed. During testing, the occurring surface strains are recorded by the optical measurement system Aramis from GOM GmbH. Since the test is not strain-controlled, slight variations in strain rate may occur. For the experiments, different strain rates were applied, whereas the testing temperature was set to 25 °C. As preparation step, the samples have to be sprayed with a stochastic pattern in the testing area. The experimental setup of the tensile test is shown in Fig. 2 b).

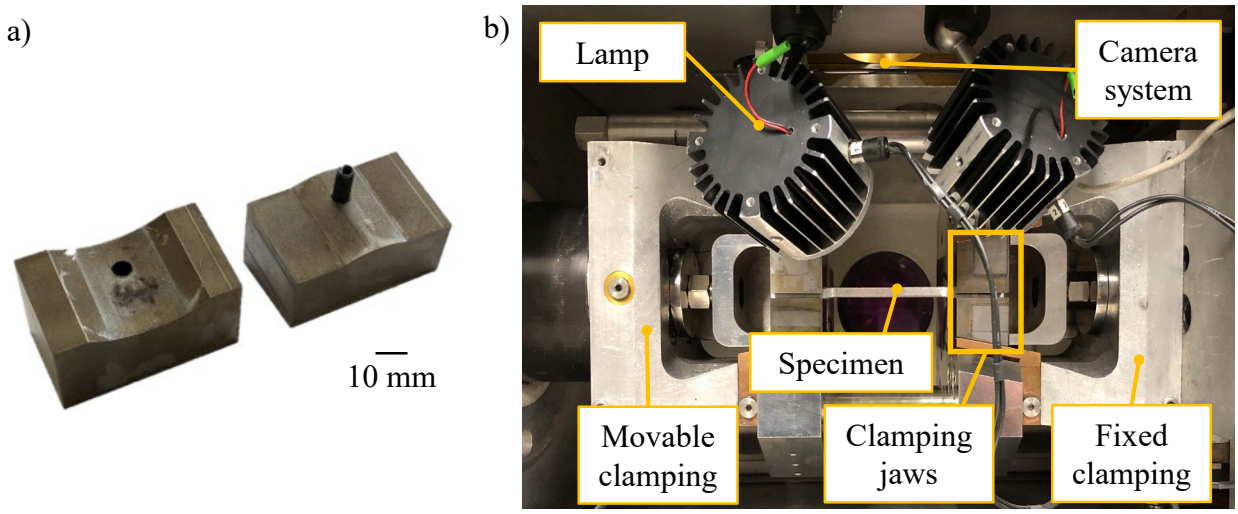

Fig. 2: a) Curved clamping jaws with integrated centering pin and b) experimental setup of the tensile test

The tensile specimen is fixed by the clamping jaws in the center of the setup. Consequently, the preload increases by moving the left side of the clamping. The position of the inner clamping jaws is fixed by u-shaped separators. In addition, conductive heat can be applied via the mounting of the clamping jaws, enabling tests at elevated temperatures. The optical strain measurement system is located above the sample, which is illuminated by two lamps.

Testing of the tensile specimens in W-temper condition. The application of cold forming processes on semi-finished parts after solution annealing and quenching is called W-temper forming. Due to the rapid cooling, microstructural transformations result in a supersaturated solid solution with a decreased strength and an improved formability [5]. Sáenz de Argandoña et al. [6] observed an enhanced formability of AA7075 in W-temper condition, which is comparable to hot forming at 300 °C. As a result of natural ageing, this state is unstable. In this context, a cold ageing duration of 45 minutes is chosen, since no significant change of the mechanical properties could be determined for the alloy AA7020 in preliminary tests in this time slot. The corresponding solution heat treatment is performed at 460 °C for 10 minutes, followed by a quenching of the samples in water.

3. Results and Discussion

3.1 Material characterization

Properties of the extruded tubular semi-finished parts in T6-temper condition. To evaluate the mechanical properties of the aluminum alloy in delivery condition T6, micro hardness measurements are carried out. These are implemented both in axial direction and across the tube cross-section using the hardness measurement system Fischerscope HM 2000 from Fischer. The hardness distribution over the cross-section is shown in Fig. 3. It is characterized by a homogenous average hardness of 140.2 HV 0.05. This observation was verified for different axial positions, indicating a uniform forming process and heat treatment. For further evaluation of the tube properties, optical measurements of the cross-sections are performed. Important results are shown in Fig. 4.

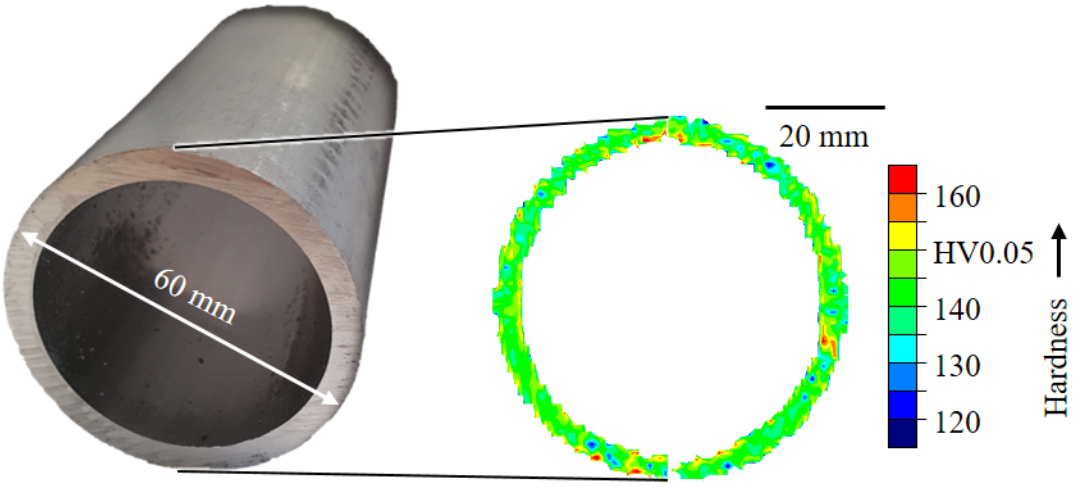

Fig. 3: Micro hardness over the tube cross-section

Fig. 4 a) shows the microstructure along the wall thickness with the outer diameter of the tube at the left and the inner diameter at the right. A significantly coarser-grained microstructure can be observed in the center compared to the surface, as shown in Fig. 4 c). Additionally, the grains are elongated in circumferential direction due to the manufacturing in an extrusion process. Significantly finer grain structures with no orientation can be found at the outer and inner diameter, whereas at the inner surface grain growth and microscopic cracks are visible. The fine fractions of the microstructure could be a result of recrystallization induced by high shear stresses and heat at the die topographies during extrusion. Consequently, no grain orientation in these sections are visible. In connection with recrystallization, grain growth might have taken place at the inner diameter, thus resulting in a thin layer with a coarse microstructure [7]. The influence of grain growth and the microscopic cracks on the mechanical properties are estimated to be low, since these only exist over a thin section of 25 µm compared to the wall thickness of five millimeters. A further indication is that only small differences of the surface roughness at the outer and inner tube diameter are visible. An average roughness at the outer surface of $R_a = 0.3946 \pm 0.0028$ µm and $R_a = 0.4577 \pm 0.0028$ µm at the inner surface was measured by a tactile measurement system.

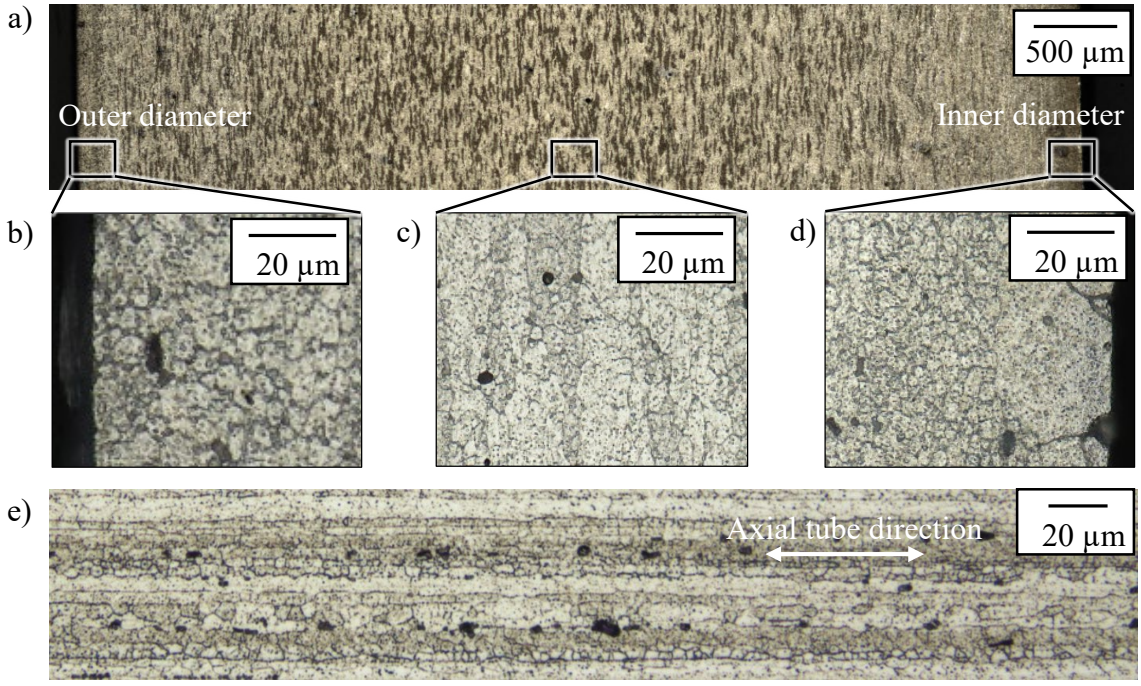

Fig. 4: a) - d) Optical characterization over the tube cross-section and e) in axial tube direction

The microstructure along the tube length in Fig. 4 e) is oriented to the extrusion direction but the grain is only slightly elongated. This might be a result of the recrystallization at the surface. In addition to the grain structure, low porosity can be seen on all micrographs. Due to the grain orientations, an anisotropic material behavior is expected.

Comparison of the mechanical properties of T6- and W-temper condition. Due to the comparatively low formability of aluminum alloys of the 7xxx series in T6-temper condition, the ductility has to be enhanced by a heat treatment. Therefore, the material is solution annealed and quenched. To verify the improvement of the formability, the mechanical properties of T6-temper and W-temper condition are compared. The flow curves for a strain rate of 0.08 s^{-1} at room temperature are shown in Fig. 5.

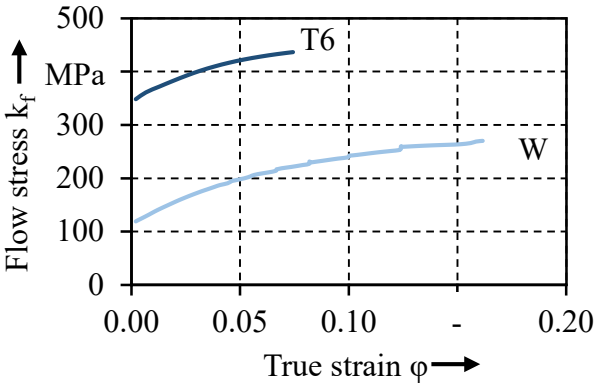

Fig. 5: Flow curves for T6- and W-temper condition

Significantly lower flow stresses are achieved in W-temper compared to T6-temper condition. In addition, the uniform elongation and strain hardening during testing is higher. For a quantitative comparison, the mechanical properties are shown in Fig. 6.

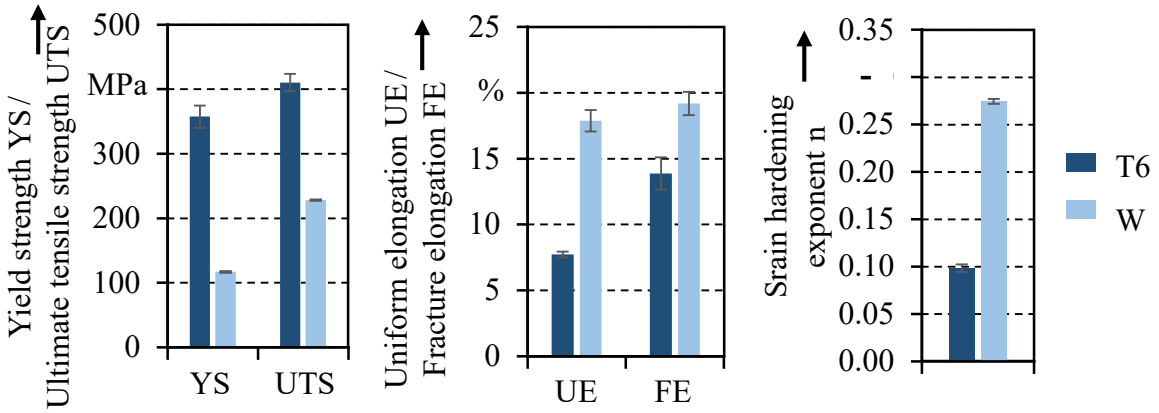

Fig. 6: Mechanical properties for T6- and W-temper condition

The yield strength in Fig. 6 for the hardened material is 357 ± 17.7 MPa, whereas the solution-annealed samples reach values around 115 ± 0.4 MPa. Furthermore, the ultimate tensile strength is 410 ± 13.6 MPa and 224 ± 1.5 MPa. W-temper forming is characterized by low flow resistance and increased ductility, which can be observed by means of the reachable strain. Besides the uniform elongation in delivery condition is 7.7 ± 0.21% and 16.8 ± 0.01% in annealed state, the elongation at fracture is 13.9 ± 1.24% and 20.5 ± 0.02%. The softened state also exhibits a significantly higher strain-hardening exponent of 0.27 ± 0.008 compared to 0.10 ± 0.004. Therefore, a further increase of formability is achieved and consequently the thinning at highly stressed areas during the forming process is reduced. Finally, W-temper forming enhances the formability, whereas this state is subsequently investigated in detail.

Investigation on strain rate sensitivity of AA7020 in W temper condition. For a deeper characterization of the mechanical properties in W-temper condition, the strain rate sensitivity is evaluated using three different strain rates. Therefore, the flow curves for the strain rates 0.01 s^{-1}, 0.08 s^{-1} and 0.90 s^{-1} are compared. These values were chosen to characterize the forming behavior of AA7020 in W-temper condition for a hydroforming process. Higher strain rates cannot be examined with the experimental setup used for the tensile tests. Fig. 7 shows exemplary experimental determined curves as well as the according to Hockett-Sherby approximated and extrapolated ones.

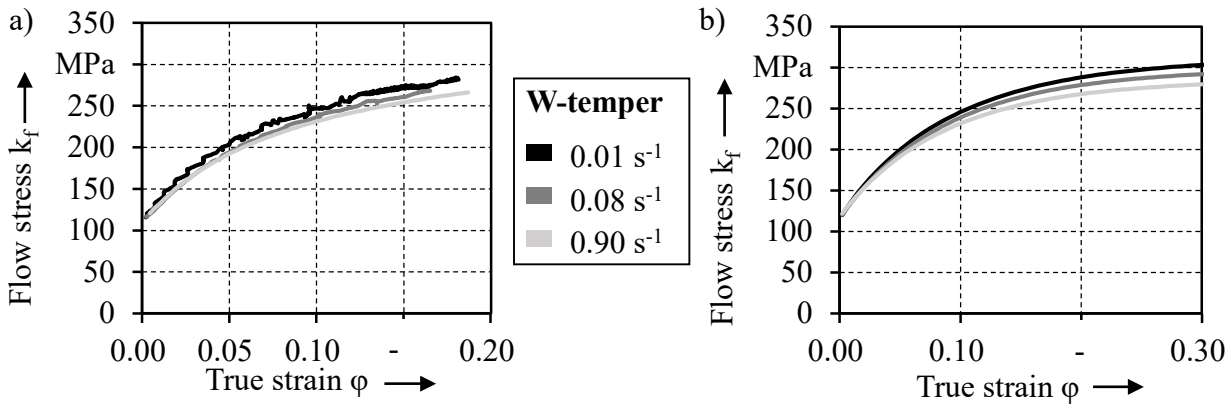

Fig. 7: a) Experimentally determined and b) approximated flow curves

For the extrapolation, all experimentally determined flow curves of each strain rate were first averaged and then approximated. The corresponding coefficients are shown in Table 1.

Table 1: Values of the flow curve approximation according to Hockett-Sherby

Equation for the flow curve approximation: $\sigma = b - (b - a) \cdot e^{-c\varphi^d}$

Strain rate [s^{-1}]	a [MPa]	b [MPa]	c	d
0.01	113.66	298.49	11.87	0.99
0.08	114.90	290.31	12.69	1.02
0.90	116.85	280.71	11.50	0.99

In general, the maximum flow stress decreases with increasing strain rate from maximum 298 MPa over 290 MPa to 281 MPa. Thus, the flow resistance declines with growing forming speed. The flow curve profile with the lowest strain rate of 0.01 s^{-1} has strong irregularities, shown in Fig. 7 a). This effect becomes weaker at a strain rate of 0.08 s^{-1} and disappears at the highest strain rate. One possible reason for this might be the Portevin-Le-Chatelier-effect (PLC-effect), which occurs mainly in AlMg alloys [7]. Thereby, the movement of the dislocations is hindered by Mg atoms. As a result, the flow stress increases to a critical value at which the dislocations break away from the barrier. Consequently, the yield stress suddenly drops, what can be observed in form of serrations in the flow curves. Due to the diffusion of Mg atoms, the deformation mechanism is hindered again, wherefore further serrations are generated. This phenomenon decreases with rising strain rates because of the time dependence of the magnesium diffusion. Thus, at high strain rates, the dislocations are not hindered by magnesium atoms anymore. As a result, the development of serrations is suppressed [7]. The impact of the PLC-effect on the mechanical properties are shown in Fig. 8.

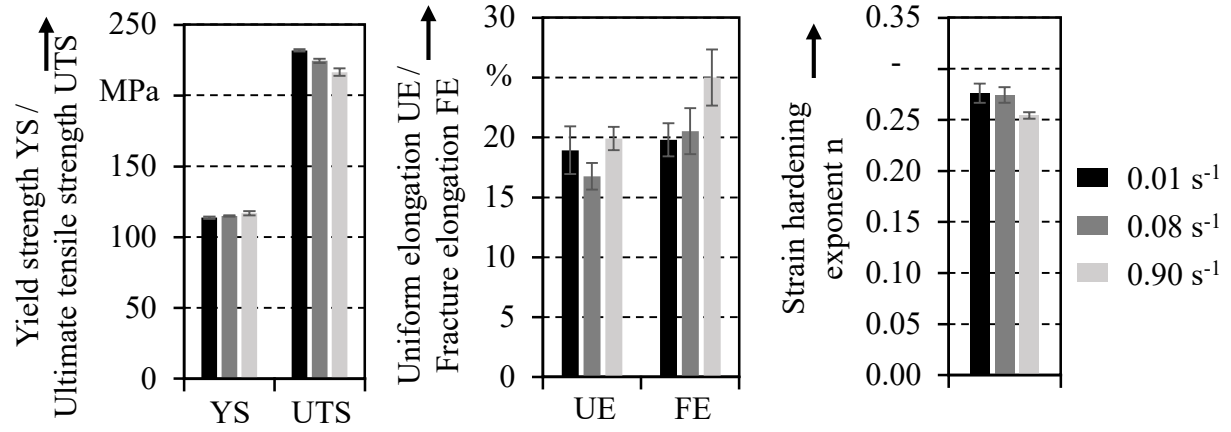

Fig. 8: Mechanical properties for different strain rates

The yield strength in Fig. 8 shows only a weak dependency from the PLC-effect with a range from 114 ± 0.8 MPa to 117 ± 1.4 MPa. On the other hand, for the ultimate tensile strength an opposite trend can be observed. It decreases with growing strain rate from 232 ± 0.8 MPa to 216 ± 2.6 MPa, this effect was already observed for the maximum flow stress. A similar behavior was described by Clausen et al. [8] for the alloy AA5083. They also detected a low increase of the yield strength whereas the maximum flow stress decreased for rising strain rates. For the aluminum alloy AA7075, Reuther et al. [9] determined a negative strain rate dependency in W-temper condition as well. In case of the uniform elongation, no clear trend is visible. However, the elongation at fracture increases with rising forming speed from 19.8 ± 1.4 % to 25.0 ± 2.3 %. The variations in the elongation may be attributed to the high wall thickness of the specimens. While the flow resistance decreases, the ductility is higher than in delivery condition. According to Halim et al. [10], the declining influence of the PLC-effect could be a reason for this. They observed a reduction of ductility for AA5754 caused by the PLC-effect. Due to the decreasing influence of the PLC-effect, the formability of the material increases for high strain rates. This behavior was also investigated by Clausen et al. [8] for AA5083. In summary, the flow stress of solution annealed AA7020 decreases with rising strain rate because of the PLC-effect, whereas the formability increases. The material data for the W-temper condition obtained from the tensile tests can subsequently be used to implement a material model in a numerical simulation. Since the setup is not suitable for the characterization of the elastic material behavior, the young's modulus is set to 70 GPa for the simulation, according to literature [11].

3.2 Model setup and FE simulation of the tensile test with tube tensile specimens

Model development and boundary conditions. To simulate the tensile test with tube tensile specimens, the associated numerical model is implemented in LS-DYNA (R12.0.0, implicit). The tube tensile specimens were discretized by a fine volume mesh according to Fig. 9 and the clamping areas were defined by nodal boundary conditions. The application of the load in the upper restraint was carried out specifying a displacement-time-curve corresponding to the averaged machine speed of the experimental tensile tests.

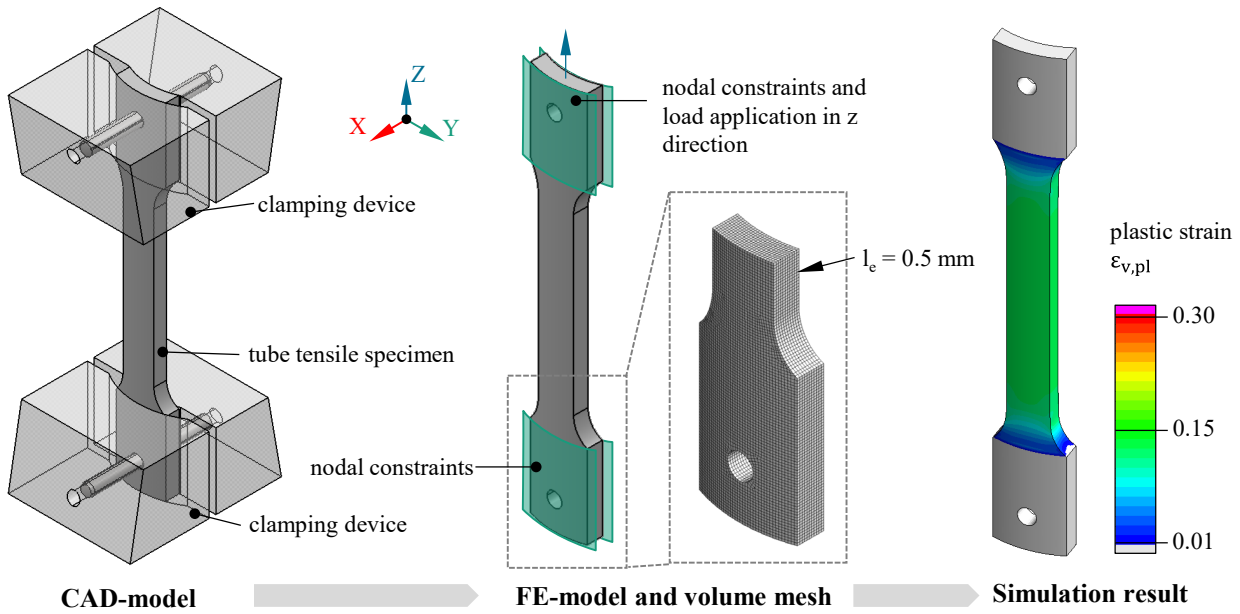

Fig. 9: Model setup of tube tensile tests with LS-DYNA

An isotropic strain rate-dependent model approach (MAT_024, MAT PIECEWISE LINEAR PLASTICITY) was selected as material model for AA7020 in W-temper condition. The flow curve approximations for the strain rates 0.01, 0.08 and 0.9 s^{-1} were stored in tabular form. For the elastic modulus, a value of 70 GPa was assumed as described in section 3.1.

Comparison of results. Three force-elongation curves of the experiments and the corresponding curve from the simulation were used as a criterion for comparison in each case, whereby in analogy to the experimental strain evaluation, a measured length of 50 mm was used as a reference length.

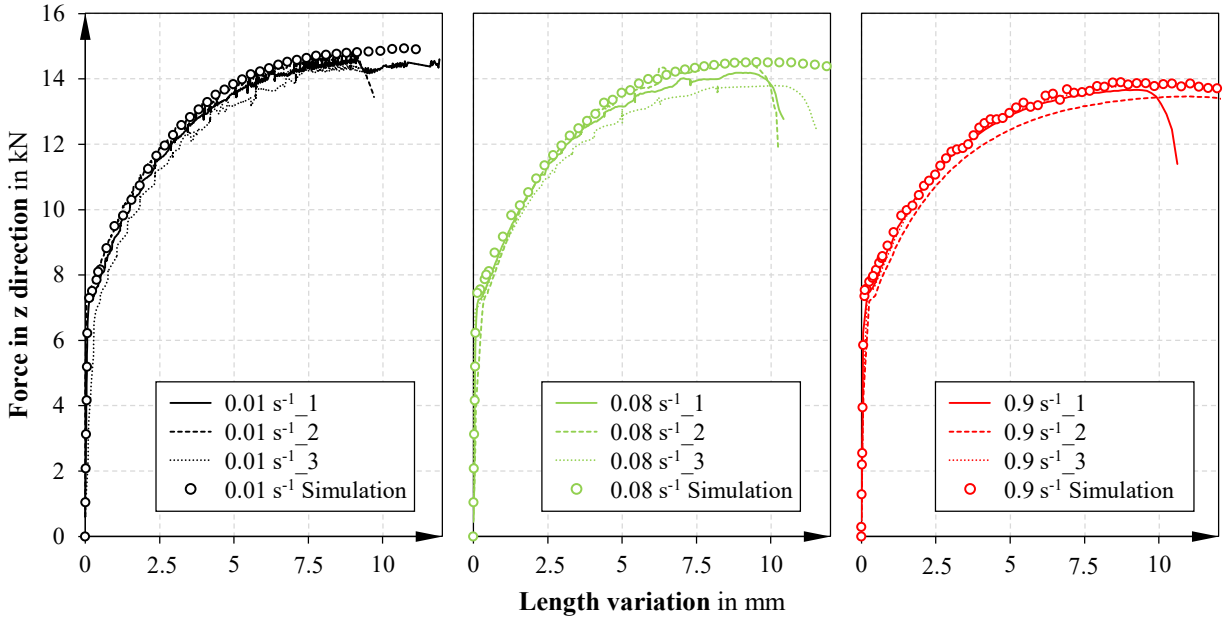

Fig. 10: Comparison of results between three experimental tube tensile tests and simulations at different discrete strain rates

The force-elongation-diagrams in Fig. 10 show a sufficient conformity of the results between simulation and experiment. The negative strain rate sensitivity caused by the PLC-effect is also correctly reproduced by the material model. Remaining differences within the results are due to the assumption of a uniform elastic modulus of 70 GPa, which leads to larger deviations primarily in the elastic zone. In addition, further inaccuracies in the zone of plastic strain can be explained by the averaging of the experimentally measured strain rates (primarily in tests with 0.08 and 0.9 s^{-1}).

As a final comparison of the simulation studies, a flat A50 tensile specimen with an equivalent cross-section and the same width was compared with the tube tensile specimen. It turned out, that using the identical material model, only minor differences result in the major and minor stress values of the tensile specimen cross-sections (differences in σ_1 and σ_2 < 0.5 MPa). In addition, the plastic strain and the testing force as a function of the elongation is investigated, as shown in Fig. 11.

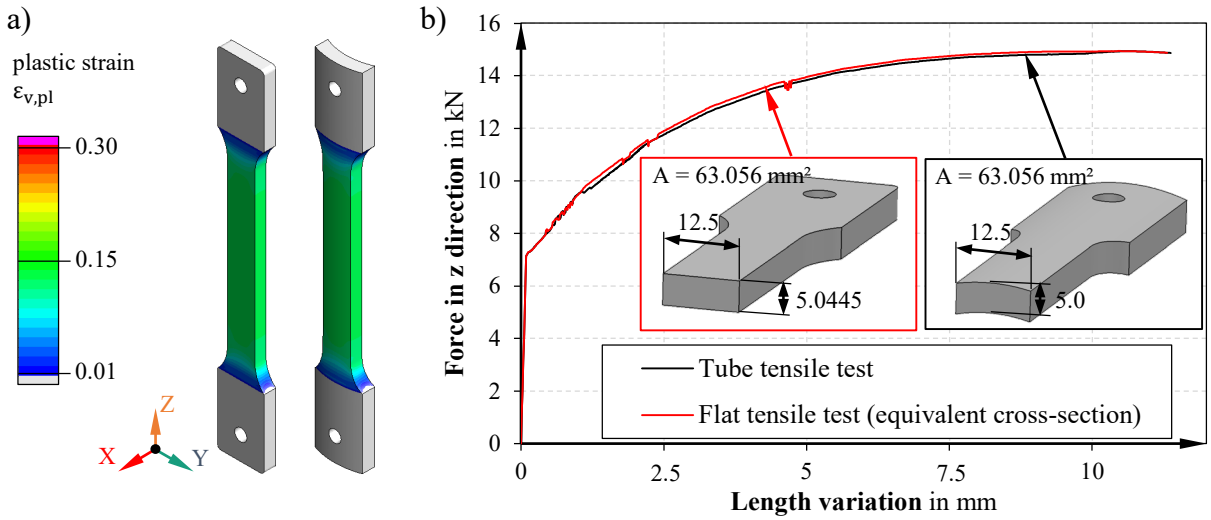

Fig.11: Comparison of a) the plastic strain and b) the testing force as a function of length variation for a flat and a curved tensile specimen at a strain rate of 0.01 s^{-1}

For the plastic strain and the testing force, no significant difference is visible. This proves that using curved clamping jaws, a comparable tensile stress and strain state can be achieved with the tube tensile specimen compared with an equivalent flat tensile specimen despite the curved cross-section.

It was shown that tubes with a wall thickness of 5 mm and a radius of 30 mm exhibit only a marginal influence in the material characterization compared to conventionally investigated flat tensile specimens. However, a stronger influence is expected as the wall thickness and the tube diameter decrease. In summary, the tensile test of curved specimen with curved clamping jaws is suitable for the experimental determination of the flow behavior in the longitudinal direction of tubes with the investigated dimensions.

4. Summary and Outlook

High strength aluminum alloys of the 7xxx series are characterized by a low ductility at room temperature. For an enhancement of the formability, the W-temper forming is applied on tubular semi-finished parts out of AA7020. To ensure the comparability of the mechanical properties determined in the tensile test, a procedure for the preparation and clamping of specimens adapted to the tube geometry was described. The samples were milled from a tube and fixed in the testing machine using curved clamping jaws. This avoids an undesired influence on the mechanical properties of the curved tensile specimens during the test. For a better evaluation of process-specific impacts of the tube extrusion on the semi-finished parts, micro hardness measurements and micrographs were analyzed. Thereby, a homogenous hardness distribution over the tube was investigated. Furthermore, orientations in the microstructure as well as recrystallization at the surfaces, caused by the heat-assisted extrusion process, were determined. To evaluate the improved formability of the annealed material, the mechanical properties in the T6 and W states were compared. In this context, an increased ductility and a decreased flow resistance were observed for the annealed material. Since the W-temper condition is more suitable for forming processes, the strain rate sensitivity was investigated for this state. For low strain rates the PLC-effect was detected, which is responsible for an increase of strength and a reduction of ductility. Consequently, a negative strain rate sensitivity was identified. By a numerical comparison of the strain and stress states between flat and curved tensile specimens during testing, no significant differences could be investigated. Therefore, the procedure for the preparation and testing of the samples is suitable for generating reliable strain rate dependent flow curves for FE simulation.

Future research should include the material testing transverse to the extrusion direction to determine the anisotropic forming behavior. This would be relevant especially for a further processing by hydroforming. Additionally, the formability of the alloy AA7020 could be analyzed at elevated temperatures. The transferability of the results regarding the stress and strain state during the testing of curved specimens on different wall thicknesses should be investigated as well.

References

[1] Information on https://ec.europa.eu/clima/eu-action/transport-emissions/road-transport-reducing-co2-emissions-vehicles/co2-emission_en , (November 17, 2021)

[2] Information on https://ec.europa.eu/clima/eu-action/transport-emissions_en, (November 17, 2021)

[3] Information on https://www.destatis.de/Europa/DE/Thema/GreenDeal/GreenDeal.html?nn=217532, (November 17, 2021)

[4] R. Neugebauer, Hydro-Umformung, Springer, Berlin, 2007.

[5] J. Degner, Grundlegende Untersuchungen zur Herstellung hochfester Aluminiumblechbauteile in einem kombinierten Umform- und Abschreckprozess, FAU University Press, Erlangen, 2020.

[6] E. Sáenz de Argandoña, L. Galdos, R. Ortubay, J. Mendiguren, X. Agirretxe, Room temperature forming of AA7075 aluminum alloys: W-temper process, Key Engineering Materials (2015).

[7] F. Ostermann, Anwendungstechnologie Aluminium, third ed., Springer Vieweg, Berlin, 2014.

[8] A.H. Clausen, T. Borvik, O.S. Hopperstad, A. Benallal, Flow and fracture characteristics of aluminium alloy AA5083-H116 as function of strain rate, temperature and triaxiality, Mater. Sci. Eng. A 364 (2004) 260–272

[9] F. Reuther, T. Lieber, J. Heidrich, V. Kräusel, Numerical Investigations on Thermal Forming Limit Testing with Local Inductive Heating for Hot Forming of AA7075,Materials 14 (2021) 1882

[10] H. Halim, D.S. Wilkinson, M. Niewczas, The Portevin-Le Chatelier (PLC) effect and shear band formation in an AA5754 alloy, Acta Materiala 55 (2007) 4151-5160

[11] M. Roth, Zur Berechnung von Bauteilen in hybrider Bauweise unter ballistischer Beanspruchung, Springer Vieweg, Berlin, 2017.